Letter

Heterogeneity induces cyclops states in Kuramoto networks with higher-mode coupling

Maxim I. Bolotov,[1] Lev A. Smirnov,[1] Vyacheslav O. Munyayev,[1] Grigory V. Osipov,[1] and Igor Belykh[2,*]

[1]*Department of Control Theory, Lobachevsky State University of Nizhny Novgorod, 23 Gagarin Avenue, Nizhny Novgorod 603022, Russia*

[2]*Department of Mathematics and Statistics and Neuroscience Institute, Georgia State University, P.O. Box 4110, Atlanta, Georgia 30302-410, USA*

(Received 14 May 2025; accepted 21 October 2025; published 14 November 2025)

Disorder is often seen as detrimental to collective dynamics, yet recent work has shown that heterogeneity can enhance network synchronization. However, its constructive role in stabilizing nontrivial cooperative patterns remains largely unexplored. In this Letter, we show that frequency heterogeneity among oscillators can induce stable cyclops and cluster states in Kuramoto networks with higher-mode coupling, even though these states are unstable in the identical oscillator case. Cyclops states, introduced in [Munyaev *et al.*, Phys. Rev. Lett. **130**, 107201 (2023)], feature two synchronized clusters and a solitary oscillator, requiring a delicate phase balance. Surprisingly, heterogeneity alone is sufficient to stabilize these patterns across a sizable range of detuning values without needing to be compensated by other forms of disorder or external tuning. To explain this effect, we introduce a mesoscopic collective coordinate approach that links microscopic frequency structure with mean-field cluster-level stability. Importantly, we demonstrate that the same disorder-induced stabilization mechanism also arises robustly in biologically and physically grounded networks of Winfree and Stuart-Landau oscillators, pointing to its generality and opening directions for designing multistate dynamics in heterogeneous networks.

DOI: 10.1103/kvyt-6gyz

Introduction. Networks of coupled phase oscillators provide a canonical framework for studying emergent behavior in complex systems [1–3]. The Kuramoto model [4–6] and its generalizations have served as central tools for understanding synchronization and related phenomena [7,8], giving rise to a wide range of collective dynamics, including full and partial synchronization [9–15], explosive synchronization [16–18], chimera patterns [19–24], solitary states [25–29], clustered states [30–33], generalized splay [34], and recently, cyclops states [35,36]. Historically, synchronization was typically studied under the assumption of identical or near-identical oscillators, treating heterogeneity and noise as disruptive. Yet, a growing body of work reveals that disorder can instead promote coherence. Frequency dispersion, delays, coupling variability, and noise have been shown to suppress spatiotemporal chaos and facilitate synchronization in a range of physical and biological systems [18,37–63]. For example, in laser oscillator arrays, added disorder in delay times can counteract the desynchronizing effects of frequency heterogeneity and restore near-perfect phase locking [64]. A particularly compelling concept is converse symmetry breaking [52,55,57–59], where the introduction of disorder enables synchronous states that are inaccessible in fully symmetric systems. For example, structural heterogeneity in the coupling topology can stabilize complete synchronization [54], and carefully tuned frequency distributions can optimize synchrony in otherwise unfavorable networks [51]. In adaptively coupled systems, the interaction of multiple disorder types, such as nodal heterogeneity and adaptive weights, can induce two distinct nonequilibrium phase transitions en route to synchrony [65]. Despite these advances, much of the prior work has focused on disorder-induced global synchronization. The ability of disorder to induce complex cooperative states, such as multicluster or other higher-dimensional cooperative dynamics, remains poorly understood, especially when such states must persist under changes in the coupling strengths or distribution of heterogeneity and without relying on additional sources of disorder or parameter fine tuning.

In this Letter, we address this conceptual knowledge gap and demonstrate that oscillator frequency heterogeneity can robustly stabilize cyclops and cluster states in the second-order Kuramoto model with higher-harmonic coupling, even though these states are unstable in networks of identical oscillators. In our previous work [35], we introduced cyclops states—a distinct class of three-cluster generalized splay states [34]—formed by two coherent clusters and a solitary oscillator with the relative phase positioned between the clusters, evocative of the Cyclops' eye. There, we showed that higher-harmonic coupling can make these states global attractors in repulsively coupled Kuramoto networks and theta-neuron models with adaptive coupling. Here, we report a counterintuitive finding that simple, nonengineered frequency heterogeneity, such as a uniform distribution, is sufficient to stabilize cyclops and related cluster states. These patterns emerge from a wide set of initial conditions and remain stable over a sizable range of oscillator heterogeneity. To explain this disorder-induced stabilization, we introduce a mesoscopic reduction based on the collective coordinate framework [65–72]. Our approach captures the interplay between microscopic frequency heterogeneity and macroscopic

*Contact author: ibelykh@gsu.edu

cluster dynamics and adopts the linear ansatz [71] to track the relative dynamics between synchronized clusters and a solitary oscillator. This formulation is particularly suited to multicluster patterns, such as cyclops states and networks with higher-mode coupling. It reveals the surprising role of disorder in transforming unstable, seemingly fragile configurations—which require a delicate phase balance—into robust and prevalent regimes. Moreover, it provides a constructive means to identify favorable ranges of heterogeneity and initial conditions that support such complex multistate dynamics.

The network model. We study a network of second-order Kuramoto-Sakaguchi oscillators with two-harmonic coupling [35,36]:

$$m\ddot{\theta}_n + \dot{\theta}_n = \omega_n + \frac{1}{N}\sum_{k=1}^{N}\sum_{q=1}^{2}\varepsilon_q \sin(q(\theta_k - \theta_n) - \alpha_q), \quad (1)$$

where $\theta_n \in [-\pi, \pi)$ is the phase of the nth oscillator, and $n = 1, \ldots, N$, with N assumed to be odd throughout the paper. The coupling function $H(\theta_k - \theta_n) = \sum_{q=1}^{2} \varepsilon_q \sin(q(\theta_k - \theta_n) - \alpha_q)$ includes first and second harmonics with strengths ε_q and phase lags $\alpha_q \in [-\pi/2, \pi/2)$, $q = 1, 2$, chosen to ensure attractive interactions with $H'(0) > 0$. Inertia is fixed at $m = 1$ to enable breathing cluster dynamics [30], which are absent in the first-order model. To highlight the generality of the disorder-induced effects, natural frequencies ω_n are drawn from a uniform distribution on $[\omega_0 - \nu, \omega_0 + \nu]$, where ν is the half-width of the distribution. No fine-tuning or engineered frequency profile is required; we take $\omega_0 = 0$ without loss of generality.

For identical oscillators with $\omega_1 = \cdots = \omega_N = \omega$, the system (1) supports cyclops states, in which the population splits into two symmetric clusters of size $K = (N-1)/2$ and a solitary oscillator. Their phases take the form $\theta_1 = \cdots = \theta_K = x + \Omega t$, $\theta_{K+1} = \cdots = \theta_{2K} = y + \Omega t$, and $\theta_N = \Omega t$, where x and y are constant phase differences relative to the nth solitary oscillator. These states are also characterized by a vanishing first-order Kuramoto order parameter $R_1(t) = \sum_{n=1}^{N} e^{i\theta_n}/N = r_1 e^{i\Theta_1}$, and a second-order parameter $R_2(t) = \sum_{n=1}^{N} e^{i2\theta_n}/N = r_2 e^{i\Theta_2}$, where $r_2 > 0$ governs their stability [34,35,73]. Two-cluster states also arise and play a central role here. They are defined by $\theta_{1..K} = \Theta_1 + \Omega t$, $\theta_{K+1..N} = \Theta_2 + \Omega t$, forming two coherent groups of unequal size in odd-N networks. This configuration is a degenerate cyclops state ($y = 0$), dynamically compensated by cluster symmetry rather than the solitary oscillator (see Fig. 1 for a direct comparison).

Depending on the coupling strengths $\varepsilon_1, \varepsilon_2$ and phase lags α_1, α_2, system (1) can support up to 16 stationary cyclops states with different ordered pairs (x, y). Their analytical forms and stability analysis in the homogeneous case ($\omega_n \equiv \omega$) were derived in [36], where cyclops states were shown to arise as dominant attractors in repulsive networks and to coexist with global synchrony under attractive coupling. These states lose stability either via an Andronov-Hopf bifurcation, leading to breathing cyclops with oscillatory $x(t), y(t)$, or through structural instabilities that produce asymmetric two-cluster states or switching cyclops, where the solitary and cluster composition change recurrently, similarly to blinking chimeras [74]. Figure 1(a) shows the corresponding stability diagram for identical oscillators, which closely parallels Fig. 8 of [36] and highlights both bifurcation scenarios. The diagram is truncated to $\alpha_2 \in [-1, 1]$ for clarity, though the existence regions extend beyond $\pm\pi/2$, where rotobreathing cyclops appear [36]. Within the cyclops region (blue), two-cluster states (white) are destabilized; two representative points are marked: a red circle (unstable cyclops) and a red cross (unstable two cluster). In the following, we show that introducing frequency heterogeneity can stabilize both regimes.

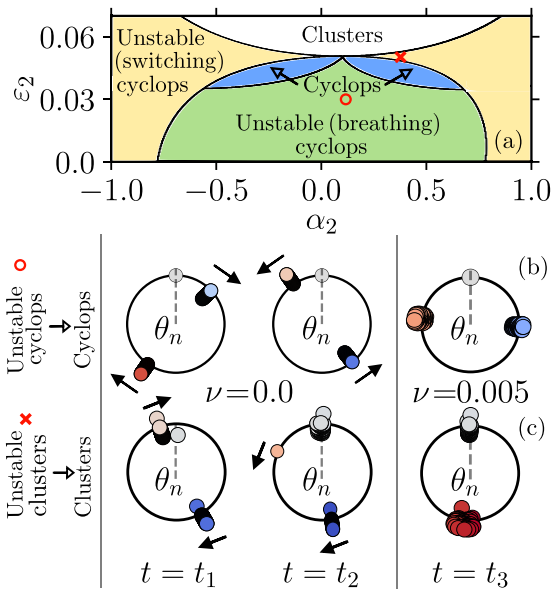

FIG. 1. Heterogeneity-induced stabilization. (a) Stability diagram for identical oscillators showing stable (blue), unstable (breathing) (green), and unstable (switching) (yellow) cyclops, and stable two-cluster states (white). Red circle ($\alpha_2 = 0.1$, $\varepsilon_2 = 0.03$) and cross ($\alpha_2 = 0.35$, $\varepsilon_2 = 0.05$) mark two representative points for unstable cyclops and cluster regimes, respectively. (b), (c) Phase snapshots (in the solitary oscillator-anchored rotating frame) comparing the identical oscillator case ($\nu = 0$, left) with the heterogeneous case ($\nu = 0.005$, right). Arrows indicate cluster oscillations; color encodes phase difference from the solitary oscillator. (b) Stabilization of unstable cyclops states at $\alpha_2 = 0.1$, $\varepsilon_2 = 0.03$. (c) Stabilization of unstable two-cluster state at $\alpha_2 = 0.35$, $\varepsilon_2 = 0.05$. Other parameters: $N = 101$, $\alpha_1 = 1.57$, $\varepsilon_1 = 1.0$.

In the presence of heterogeneous frequencies ω_n, the perfectly symmetric cyclops and two-cluster states of the identical-oscillator case no longer exist, but their analogs can still be defined. In a heterogeneous cyclops state, phases within each cluster are no longer identical yet remain tightly grouped. Specifically, we write $\theta_n(t) = \varphi_n + \theta_N(t)$, where φ_n denotes the nth oscillator's relative phase with respect to the solitary unit ($\varphi_N = 0$). Within each cluster, relative phase differences satisfy $|\varphi_j - \varphi_k| = C_{jk} < \pi$ for all $j, k \in 1, \ldots, K$ or $j, k \in K+1, \ldots, 2K$, enforcing a phase bound that prevents phase slips and cluster overlap. Similarly, in a heterogeneous two-cluster state, phases satisfy $\theta_n(t) = \varphi_n + \Omega t$ with bounded intracluster differences $|\varphi_j - \varphi_k| = C_{jk} < \pi$.

Heterogeneity-induced effects. Figures 1(b) and 1(c) show that introducing frequency heterogeneity with $\nu = 0.005$

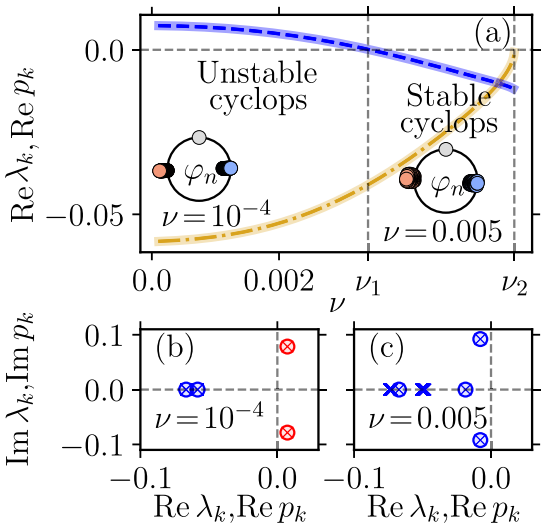

FIG. 2. Stabilization of the cyclops state by frequency heterogeneity for the parameter set corresponding to the red circle in Fig. 1(a). (a) Real parts of the leading eigenvalues of the full system (2) (λ_k; dashed and dash-dotted lines) and the reduced model (4) (p_k; solid transparent lines). Blue curves: complex-conjugate eigenvalues $\lambda_{1,2}$, $p_{1,2}$ controlling stability; yellow curves: real eigenvalues λ_3, p_3 associated with existence. Stability is achieved for $\nu \in [\nu_1, \nu_2] \approx [0.0034, 0.0057]$, after which the cyclops state disappears. Insets: phase snapshots of the corresponding cyclops states (unstable at $\nu = 10^{-4}$ and stable at $\nu = 0.005$). (b), (c) Comparison of individual eigenvalues at $\nu = 10^{-4}$ (b) and $\nu = 0.005$ (c); crosses: full model (λ_k), circles: reduced model (p_k). Blue: stable; red: unstable. Only eigenvalues near the imaginary axis are shown. Parameters: $N = 101$, $\alpha_1 = 1.57$, $\varepsilon_1 = 1.0$, $\alpha_2 = 0.1$, $\varepsilon_2 = 0.03$.

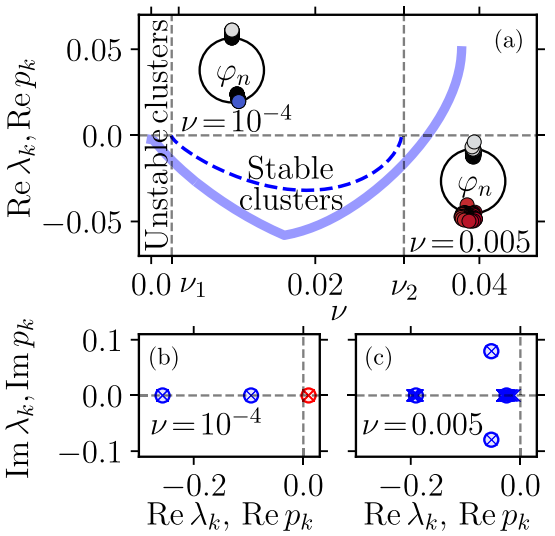

FIG. 3. Stabilization of the two-cluster state by frequency heterogeneity for the parameter set corresponding to the red cross in Fig. 1(a). (a) Real parts of the leading eigenvalue of the full system (2) (λ_1; dashed line) and reduced model (4) (p_1; solid transparent line). Blue curves: λ_1 and p_1, which govern the stability of the two-cluster state. Stability emerges in the interval $\nu \in [\nu_1, \nu_2] \approx [0.00244, 0.0305]$. Insets: phase snapshots of the corresponding two-cluster regimes (unstable at $\nu = 10^{-4}$ and stable at $\nu = 0.005$). (b), (c) Comparison of eigenvalues at $\nu = 10^{-4}$ (b) and $\nu = 0.005$ (c); crosses: full model (λ_k), circles: reduced model (p_k). Blue: stable; red: unstable. Only eigenvalues near the imaginary axis are shown. Parameters: $N = 101$, $\alpha_1 = 1.57$, $\varepsilon_1 = 1.0$, $\alpha_2 = 0.35$, $\varepsilon_2 = 0.05$.

stabilizes previously unstable cyclops and two-cluster states [red markers in Fig. 1(a)]. Supplemental Material Movies 1 and 2 [75] illustrate the full dynamics of this stabilization process. The mechanism behind this effect can be understood as follows. In the identical oscillator case, the cyclops state requires each oscillator within a cluster to maintain a fixed phase difference (x or y) relative to the solitary oscillator. Any deviation from this strict phase alignment may disrupt the cluster structure and destabilize the cyclops state as a whole. Frequency heterogeneity, however, introduces small intracluster phase variations, broadening the clusters' phase width. While one might expect this to further disrupt the balance required for cyclops formation, the internal phase shifts instead contribute to a compensating effect: oscillators with slightly larger or smaller phase differences balance each other out, allowing the cluster-average phase to satisfy the required condition relative to the solitary node. Thus, the heterogeneity among oscillators directly induces a stable cyclops state [Fig. 1(b)]. A similar mechanism applies to the stabilization of two-cluster states, where broadened clusters maintain a constant average phase separation. Strictly speaking, heterogeneity does not stabilize the perfectly symmetric states of the identical oscillator system but instead gives rise to structurally similar configurations with nonzero intra-cluster phase spreads. Figure 2 shows that increasing ν initially produces an unstable cyclops state with tightly grouped oscillators; further increase stabilizes it over a broad range $\nu \in [\nu_1, \nu_2]$. Similarly, Fig. 3 demonstrates that for the two-cluster regime, small ν first destroys the unstable two-cluster symmetric state at $\nu = 0$, then induces a misaligned two-cluster configuration, which remains stable over $\nu \in [\nu_1, \nu_2]$.

Reduction via collective coordinates. To track the evolution of relative phase differences $\varphi_n = \theta_n - \theta_N$ with respect to the solitary oscillator, we transform the original system (1) into the phase difference system for $n = 1, \ldots, N-1$. Using the identity $\sin\phi = \mathrm{Im}[e^{i\phi}]$, we write the phase difference system compactly in complex form:

$$m\ddot{\varphi}_n + \dot{\varphi}_n = \Delta_n + \sum_{q=1}^{2} \mathrm{Im}\left[\frac{\varepsilon_q e^{-i\alpha_q}}{N}\left(\sum_{k=1}^{N-1} e^{iq\varphi_k} + 1\right)(e^{-iq\varphi_n} - 1)\right], \tag{2}$$

where $\Delta_n = \omega_n - \omega_N$ is the detuning relative to the solitary oscillator. Stable fixed points of Eq. (2) correspond to stable distributions of constant relative phases φ_n, including cyclops states and two-cluster configurations.

Directly identifying such states in large heterogeneous networks is computationally demanding and often elusive. To address this, we employ a mesoscopic reduction via the collective coordinate approach [65–72]. Given uniformly distributed natural frequencies ω_n, we approximate the phase profile within each cluster by a linear ansatz:

$$\begin{aligned} \varphi_n(t) &\approx \hat{\varphi}_n(t) = \psi_1(t) + \chi_1(t)\Delta_n, \quad n = 1, \ldots, K, \\ \varphi_n(t) &\approx \hat{\varphi}_n(t) = \psi_2(t) + \chi_2(t)\Delta_n, \quad n = K+1, \ldots, 2K, \end{aligned} \tag{3}$$

where $\psi_\mu(t)$ represents the average phase of cluster $\mu = 1, 2$, and $\chi_\mu(t)$ describes the phase drift within each cluster. The product $\chi_\mu(t)\Delta_n$ accounts for deviations from the collective phase due to oscillator detuning. In simple terms, the ansatz expresses each oscillator's phase as the sum of a macroscopic cluster phase and a frequency-dependent drift. This drift captures the microscopic frequency-induced spread of phases within each cluster, relative to the solitary oscillator, yielding a mesoscopic description of the collective dynamics.

Following the collective coordinate approach [71], we substitute the ansatz into Eq. (2), and we compute the residual (error vector) between the exact and approximate dynamics. The evolution equations for the collective coordinates are obtained by requiring this residual to be orthogonal to the tangent space of the ansatz manifold, spanned by the gradients $\partial\hat{\varphi}_n/\partial\psi_\mu$ and $\partial\hat{\varphi}_n/\partial\chi_\mu$. This Galerkin projection yields the closed system (4), governing the evolution of mesoscopic cluster parameters under heterogeneous detuning. Full derivation details are provided in the Supplemental Material [75]. These equations for $\psi_\mu(t)$ and $\chi_\mu(t)$ approximate the macroscopic evolution of cluster-averaged phase positions and internal phase spreads in a finite oscillator network with heterogeneous detuning values Δ_n:

$$\begin{aligned} m\ddot{\psi}_\mu + \dot{\psi}_\mu &= \sum_{q=1}^{2} \mathrm{Im}\Bigg[\frac{\varepsilon_q e^{-i\alpha_q}}{N}\big(1 + KS_1^{(q)}e^{iq\psi_1} \\ &\quad + KS_2^{(q)}e^{iq\psi_2}\big)\Bigg(\frac{\sigma_\mu^2 S_\mu^{(q)^*} - \delta_\mu J_\mu^{(q)^*}}{\sigma_\mu^2 - \delta_\mu^2}e^{-iq\psi_\mu} - 1\Bigg)\Bigg], \\ m\ddot{\chi}_\mu + \dot{\chi}_\mu &= 1 + \frac{1}{\sigma_\mu^2 + \delta_\mu^2}\sum_{q=1}^{2} \mathrm{Im}\Bigg[\frac{\varepsilon_q e^{-i\alpha_q}}{N}\big(1 + KS_1^{(q)}e^{iq\psi_1} \\ &\quad + KS_2^{(q)}e^{iq\psi_2}\big)\big(J_\mu^{(q)^*} - \delta_\mu S_\mu^{(q)^*}\big)e^{-iq\psi_\mu}\Bigg], \end{aligned} \tag{4}$$

$$\delta_\mu = \sum_{k=(\mu-1)K+1}^{\mu K} \Delta_k \Big/ K, \quad S_\mu^{(q)} = \sum_{k=(\mu-1)K+1}^{\mu K} e^{iq\chi_\mu\Delta_k} \Big/ K, \tag{5}$$

$$\sigma_\mu^2 = \sum_{k=(\mu-1)K+1}^{\mu K} \Delta_k^2 \Big/ K, \quad J_\mu^{(q)} = \sum_{k=(\mu-1)K+1}^{\mu K} \Delta_k e^{iq\chi_\mu\Delta_k} \Big/ K, \tag{6}$$

where δ_μ is the average frequency detuning, σ_μ^2 is the second moment of the frequency distribution, $S_\mu^{(q)}$ is the qth order parameter of phase deviations from the average collective phase, and $J_\mu^{(q)}$ is the corresponding frequency-weighted order parameter, all computed within the μth cluster. Stationary solutions of the reduced system (4), given by vector $\mathbf{\Gamma}^* = (\psi_1^*, \psi_2^*, \chi_1^*, \chi_2^*)$, can be used to reconstruct cyclops states of the full system (2) via the ansatz (3), offering a computationally efficient way to identify candidate cyclops configurations. As shown in Fig. 1 in the Supplemental Material [75], the agreement between the reduced and full models is remarkably close, with deviations on the order of 10^{-3} for typical parameter values. Once candidate cyclops states are identified via the stationary solutions $\mathbf{\Gamma}^*$, their linear stability can be readily assessed. This is done by evaluating the eigenvalues $p_1, \ldots, p_8$ of the linearized eight-dimensional system around $\mathbf{\Gamma}^*$, derived from Eq. (4) (see the Supplemental Material [75]). These eigenvalues determine the local stability of the reduced mesoscopic dynamics and serve as a computationally efficient proxy for the full system, whose Jacobian has $2(N-1)$ eigenvalues $\lambda_1, \ldots, \lambda_{2(N-1)}$. Figure 2 shows that the eigenvalues λ_k of the full system (2) and p_k of the reduced model (4) match remarkably well, confirming the predictive accuracy of the mesoscopic approach. In particular, the blue curves in Fig. 2(a) show that the leading complex-conjugate eigenvalue pairs $(\lambda_{1,2})$ and $(p_{1,2})$, which govern the stability of the cyclops state, evolve nearly identically in both models as ν varies.

The reduced system (4) also applies to two-cluster states, which, unlike cyclops states, do not involve a solitary oscillator. In this case, all relative phases can be defined with respect to a common zero reference phase, and the nth oscillator is simply included in one of the two clusters. While the reduced system (4) provides a close match to the two-cluster phase distributions observed in the full system, its eigenvalue predictions are less accurate. Figure 3 shows good agreement near the stability boundaries, slightly below [Fig. 3(b)] and just above [Fig. 3(c)] the stabilization onset at ν_1 but the correspondence degrades toward the middle of the stable $\nu \in [\nu_1, \nu_2]$ interval. Both cyclops and two-cluster states induced by frequency heterogeneity possess sizable basins of attraction (Fig. 2 in the Supplemental Material) [75]. For intermediate two-cluster initial phase spreads, the system converges to stationary regimes with high probability, up to 70% for two-cluster states and up to 40% for cyclops states, even though the solitary oscillator is absent from the initial conditions. At the same time, in the remaining realizations, it evolves into multicluster or switching states.

Beyond Kuramoto networks. To demonstrate the generality of heterogeneity-induced stabilization in more biologically relevant settings, we consider a globally coupled Winfree network [76,77] (a canonical neuronal model) with two-harmonic phase response and narrow pulse coupling. Each oscillator evolves as $\dot{\theta}_n = \omega_n + Q(\theta_n)\frac{\kappa}{N}\sum_{k=1}^{N} P(\theta_k)$, where $\omega_n \in [\omega_0 - \nu, \omega_0 + \nu]$. The sensitivity function is $Q(\vartheta) = \varsigma_0 + \varsigma_1\sin(\vartheta + \beta_1) + \varsigma_2\sin(2\vartheta + \beta_2)$, and the pulse function is $P(\vartheta) = p_s(1 + \cos\vartheta)^s$ with $s = 20$ (narrow pulses) and p_s normalized so that $\int_0^{2\pi} P(\vartheta)\,d\vartheta = 2\pi$.

Figure 4(a) demonstrates the emergence of a dominant breathing cyclops state in the identical Winfree oscillator network with $\nu = 0$. Because Winfree oscillators inherently spike, the state combines small-amplitude, high-frequency oscillations within clusters with slow, large-amplitude intercluster modulations—closely paralleling the breathing cyclops observed in the Kuramoto case [Fig. 1(b)]. The order parameter r_1 thus displays clear two-time scale oscillations around zero. Introducing even slight heterogeneity ($\nu = 5 \times 10^{-4}$) suppresses the slow intercluster dynamics, effectively acting as a low-pass filter on the macroscopic signal. The network then stabilizes into two dominant, nonbreathing patterns: either a cyclops state or a two-cluster state [Figs. 4(b) and 4(c)]. Both stabilized regimes, observed separately in the Kuramoto model, now emerge robustly from random initial conditions, underscoring the generality of the effect. Beyond

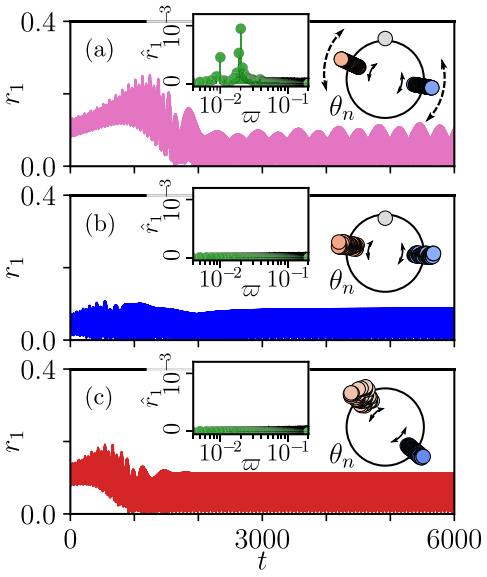

FIG. 4. Heterogeneity-induced stabilization in the Winfree network. Dynamics of the order parameter $r_1 = |\frac{1}{N}\sum_{k=1}^{N} e^{i\theta_k}|$ for (a) a breathing cyclops state ($\mathcal{P} = 1.0$, $\nu = 0.0$), (b) a nonbreathing cyclops state ($\mathcal{P} = 0.27$, $\nu = 5 \times 10^{-4}$), and (c) a two-cluster state ($\mathcal{P} = 0.73$, $\nu = 5 \times 10^{-4}$). Probabilities $\mathcal{P}$ quantify the fraction of runs converging to each state, estimated over 100 trials with random initial phases uniformly distributed in $[-\pi, \pi]$. Left insets: low-frequency power spectrum of $r_1(t)$ (ϖ: frequency, $\hat{r}_1$: magnitude). Note the disappearance of the low-frequency peaks under heterogeneity. Right insets: final phase distributions θ_n. Dotted arrows highlight large-amplitude, low-frequency intercluster oscillations; solid arrows mark small-amplitude, high-frequency intracluster oscillations. Parameters: $N = 101$, $\omega_0 = 3.0$, $\kappa = 1.0$, $\varsigma_0 = 0.0$, $\varsigma_1 = 0.13125$, $\varsigma_2 = -0.00456$, $\beta_1 = 1.57$, $\beta_2 = 0.1$.

phase models, the stabilization mechanism also robustly manifests in networks of Stuart-Landau oscillators, widely used in laser physics [78], under higher-order coupling (Fig. 3 in the Supplemental Material [75]).

Conclusions. We have revealed a counterintuitive effect whereby oscillator frequency heterogeneity can stabilize cyclops and cluster states that are unstable in identical-oscillator networks. This disorder-induced mechanism transforms configurations that would otherwise require precise phase balance into robust, dynamically accessible regimes across a broad range of initial conditions and heterogeneity sizes. Using a simple uniform frequency distribution, without fine tuning, we demonstrated that heterogeneity alone can induce stability. Beyond Kuramoto networks, we showed that the same mechanism arises in Winfree and Stuart-Landau oscillators, extending its relevance to biologically and physically grounded systems. These results demonstrate that stabilization of multicluster dynamics stems from the interplay between higher-order coupling and frequency heterogeneity, rather than model-specific details. Since Winfree oscillators are equivalent to canonical theta neurons under transformation [79–82], we expect this stabilization mechanism, where frequency heterogeneity acts as a macroscopic low-pass filter, to emerge in heterogeneous neuronal circuits broadly.

Acknowledgments. This work was supported by the Russian Science Foundation under Project No. 24-72-00105 (to M.I.B.), the MSHE under Project No. FSWR-2020-0036 (to V.O.M., L.A.S., and G.V.O., Supplemental Material [75]), and the National Science Foundation (USA) under Grant DMS-2510860 and the Georgia State University Brain and Behavior Program (to I.B.).

Data availability. The data that support the findings of this article are not publicly available. The data are available from the authors upon reasonable request.

[1] F. C. Hoppensteadt and E. M. Izhikevich, *Weakly Connected Neural Networks* (Springer Science & Business Media, New York, USA, 2012), Vol. 126.
[2] M. R. Tinsley, S. Nkomo, and K. Showalter, Nat. Phys. **8**, 662 (2012).
[3] A. E. Motter, S. A. Myers, M. Anghel, and T. Nishikawa, Nat. Phys. **9**, 191 (2013).
[4] Y. Kuramoto, in *International Symposium on Mathematical Problems in Theoretical Physics* (Springer, Kyoto, Japan, 1975), pp. 420–422.
[5] S. H. Strogatz, Physica D **143**, 1 (2000).
[6] S. Crook, G. Ermentrout, M. Vanier, and J. M. Bower, J. Comput. Neurosci. **4**, 161 (1997).
[7] J. A. Acebrón, L. L. Bonilla, C. J. P. Vicente, F. Ritort, and R. Spigler, Rev. Mod. Phys. **77**, 137 (2005).
[8] E. Ott and T. M. Antonsen, Chaos **18**, 037113 (2008).
[9] H.-A. Tanaka, A. J. Lichtenberg, and S. Oishi, Phys. Rev. Lett. **78**, 2104 (1997).
[10] H.-A. Tanaka, A. J. Lichtenberg, and S. Oishi, Physica D **100**, 279 (1997).
[11] P. Ji, T. K. Peron, F. A. Rodrigues, and J. Kurths, Sci. Rep. **4**, 6292 (2014).
[12] V. Munyaev, L. Smirnov, V. Kostin, G. Osipov, and A. Pikovsky, New J. Phys. **22**, 023036 (2020).
[13] M. Komarov, S. Gupta, and A. Pikovsky, EPL (Europhysics Letters) **106**, 40003 (2014).
[14] E. A. Martens, E. Barreto, S. H. Strogatz, E. Ott, P. So, and T. M. Antonsen, Phys. Rev. E **79**, 026204 (2009).
[15] N. V. Barabash, V. N. Belykh, G. V. Osipov, and I. V. Belykh, Chaos **31**, 113113 (2021).
[16] J. Gómez-Gardenes, S. Gómez, A. Arenas, and Y. Moreno, Phys. Rev. Lett. **106**, 128701 (2011).
[17] P. Ji, T. K. DM. Peron, P. J. Menck, F. A. Rodrigues, and J. Kurths, Phys. Rev. Lett. **110**, 218701 (2013).
[18] P. S. Skardal and A. Arenas, Phys. Rev. E **89**, 062811 (2014).
[19] Y. Kuramoto and D. Battogtokh, Nonlinear Phenom. Complex Syst. **5**, 380 (2002).
[20] D. M. Abrams and S. H. Strogatz, Phys. Rev. Lett. **93**, 174102 (2004).

[21] D. M. Abrams, R. Mirollo, S. H. Strogatz, and D. A. Wiley, Phys. Rev. Lett. **101**, 084103 (2008).
[22] M. J. Panaggio and D. M. Abrams, Nonlinearity **28**, R67 (2015).
[23] M. I. Bolotov, G. V. Osipov, and A. Pikovsky, Phys. Rev. E **93**, 032202 (2016).
[24] M. Bolotov, L. Smirnov, G. Osipov, and A. Pikovsky, Chaos **28**, 045101 (2018).
[25] P. Jaros, Y. Maistrenko, and T. Kapitaniak, Phys. Rev. E **91**, 022907 (2015).
[26] Y. Maistrenko, S. Brezetsky, P. Jaros, R. Levchenko, and T. Kapitaniak, Phys. Rev. E **95**, 010203(R) (2017).
[27] P. Jaros, S. Brezetsky, R. Levchenko, D. Dudkowski, T. Kapitaniak, and Y. Maistrenko, Chaos **28**, 011103 (2018).
[28] E. Teichmann and M. Rosenblum, Chaos **29**, 093124 (2019).
[29] V. O. Munyayev, M. I. Bolotov, L. A. Smirnov, G. V. Osipov, and I. V. Belykh, Phys. Rev. E **105**, 024203 (2022).
[30] I. V. Belykh, B. N. Brister, and V. N. Belykh, Chaos **26**, 094822 (2016).
[31] B. N. Brister, V. N. Belykh, and I. V. Belykh, Phys. Rev. E **101**, 062206 (2020).
[32] R. Ronge and M. A. Zaks, Eur. Phys. J.: Spec. Top. **230**, 2717 (2021).
[33] Y. Zhang and A. E. Motter, SIAM Rev. **62**, 817 (2020).
[34] R. Berner, S. Yanchuk, Y. Maistrenko, and E. Scholl, Chaos **31**, 073128 (2021).
[35] V. O. Munyayev, M. I. Bolotov, L. A. Smirnov, G. V. Osipov, and I. Belykh, Phys. Rev. Lett. **130**, 107201 (2023).
[36] M. I. Bolotov, V. O. Munyayev, L. A. Smirnov, G. V. Osipov, and I. Belykh, Phys. Rev. E **109**, 054202 (2024).
[37] Y. Braiman, J. F. Lindner, and W. L. Ditto, Nature (London) **378**, 465 (1995).
[38] Y. Braiman, W. Ditto, K. Wiesenfeld, and M. Spano, Phys. Lett. A **206**, 54 (1995).
[39] F. Qi, Z. Hou, and H. Xin, Phys. Rev. Lett. **91**, 064102 (2003).
[40] Á. Corral, C. J. Pérez, and A. Díaz-Guilera, Phys. Rev. Lett. **78**, 1492 (1997).
[41] A. Neiman, L. Schimansky-Geier, A. Cornell-Bell, and F. Moss, Phys. Rev. Lett. **83**, 4896 (1999).
[42] N. V. Alexeeva, I. V. Barashenkov, and G. P. Tsironis, Phys. Rev. Lett. **84**, 3053 (2000).
[43] A. Gavrielides, T. Kottos, V. Kovanis, and G. P. Tsironis, Phys. Rev. E **58**, 5529 (1998).
[44] Y. Braiman, H. G. E. Hentschel, F. Family, C. Mak, and J. Krim, Phys. Rev. E **59**, R4737 (1999).
[45] G. V. Osipov and M. M. Sushchik, Phys. Rev. E **58**, 7198 (1998).
[46] L. L. Rubchinsky, M. Sushchik, and G. V. Osipov, Math. Comput. Simul. **58**, 443 (2002).
[47] S. F. Brandt, B. K. Dellen, and R. Wessel, Phys. Rev. Lett. **96**, 034104 (2006).
[48] G. Montaseri and M. Meyer-Hermann, Phys. Rev. E **94**, 042213 (2016).
[49] Y.-Y. Li, B. Jia, H.-G. Gu, and S.-C. An, Commun. Theor. Phys. **57**, 817 (2012).
[50] C. J. Tessone, C. R. Mirasso, R. Toral, and J. D. Gunton, Phys. Rev. Lett. **97**, 194101 (2006).
[51] D. Taylor, P. S. Skardal, and J. Sun, SIAM J. Appl. Math. **76**, 1984 (2016).
[52] T. Nishikawa and A. E. Motter, Phys. Rev. Lett. **117**, 114101 (2016).
[53] I. Belykh, R. Jeter, and V. Belykh, Sci. Adv. **3**, e1701512 (2017).
[54] J. D. Hart, Y. Zhang, R. Roy, and A. E. Motter, Phys. Rev. Lett. **122**, 058301 (2019).
[55] Z. G. Nicolaou, D. Eroglu, and A. E. Motter, Phys. Rev. X **9**, 011017 (2019).
[56] Z. G. Nicolaou, M. Sebek, I. Z. Kiss, and A. E. Motter, Phys. Rev. Lett. **125**, 094101 (2020).
[57] F. Molnar, T. Nishikawa, and A. E. Motter, Nat. Phys. **16**, 351 (2020).
[58] Y. Zhang, J. L. Ocampo-Espindola, I. Z. Kiss, and A. E. Motter, Proc. Natl. Acad. Sci. USA **118**, e2024299118 (2021).
[59] F. Molnar, T. Nishikawa, and A. E. Motter, Nat. Commun. **12**, 1457 (2021).
[60] N. Punetha and L. Wetzel, Phys. Rev. E **106**, L052201 (2022).
[61] Y. Sugitani, Y. Zhang, and A. E. Motter, Phys. Rev. Lett. **126**, 164101 (2021).
[62] Y. Eliezer, S. Mahler, A. A. Friesem, H. Cao, and N. Davidson, Phys. Rev. Lett. **128**, 143901 (2022).
[63] M. Honari-Latifpour, J. Ding, I. Belykh, and M.-A. Miri, Chaos **35**, 021101 (2025).
[64] N. Nair, K. Hu, M. Berrill, K. Wiesenfeld, and Y. Braiman, Phys. Rev. Lett. **127**, 173901 (2021).
[65] J. Fialkowski, S. Yanchuk, I. M. Sokolov, E. Schöll, G. A. Gottwald, and R. Berner, Phys. Rev. Lett. **130**, 067402 (2023).
[66] S. M. Cox and G. A. Gottwald, Physica D **216**, 307 (2006).
[67] G. A. Gottwald, Chaos **25**, 053111 (2015).
[68] E. J. Hancock and G. A. Gottwald, Phys. Rev. E **98**, 012307 (2018).
[69] L. D. Smith and G. A. Gottwald, Chaos **29**, 093127 (2019).
[70] R. Berner, A. Lu, and I. M. Sokolov, Chaos **33**, 073138 (2023).
[71] L. D. Smith and G. A. Gottwald, Chaos **30**, 093107 (2020).
[72] A. Yadav, J. Fialkowski, R. Berner, V. K. Chandrasekar, and D. V. Senthilkumar, Phys. Rev. E **109**, L052301 (2024).
[73] P. S. Skardal, E. Ott, and J. G. Restrepo, Phys. Rev. E **84**, 036208 (2011).
[74] R. J. Goldschmidt, A. Pikovsky, and A. Politi, Chaos **29**, 071101 (2019).
[75] See Supplemental Material at http://link.aps.org/supplemental/10.1103/kvyt-6gyz for derivations and other details as well as two videos.
[76] A. T. Winfree, J. Theor. Biol. **16**, 15 (1967).
[77] D. Pazó and E. Montbrió, Phys. Rev. X **4**, 011009 (2014).
[78] L. Jaurigue, E. Schöll, and K. Lüdge, Phys. Rev. Lett. **117**, 154101 (2016).
[79] G. B. Ermentrout and N. Kopell, SIAM J. Appl. Math. **46**, 233 (1986).
[80] B. S. Gutkin and G. B. Ermentrout, Neural Comput. **10**, 1047 (1998).
[81] P. So, T. B. Luke, and E. Barreto, Physica D **267**, 16 (2014).
[82] L. A. Smirnov, V. O. Munyayev, M. I. Bolotov, G. V. Osipov, and I. Belykh, Front. Netw. Physiol. **4**, 1423023 (2024).